

Landslides (2017) 14:685–696
 DOI 10.1007/s10346-016-0767-6
 Received: 10 May 2016
 Accepted: 10 October 2016
 Published online: 4 November 2016
 © The Author(s) 2016
 This article is published with open access
 at Springerlink.com

Luca Lombardi · Massimiliano Nocentini · William Frodella · Teresa Nolesini · Federica Bardi · Emanuele Intrieri · Tommaso Carlà · Lorenzo Solari · Giulia Dotta · Federica Ferrigno · Nicola Casagli

The Calatabiano landslide (southern Italy): preliminary GB-InSAR monitoring data and remote 3D mapping

Abstract On 24 October 2015, following a period of heavy rainfall, a landslide occurred in the Calatabiano Municipality (Sicily Island, Southern Italy), causing the rupture of a water pipeline supplying water to the city of Messina. Following this event, approximately 250,000 inhabitants of the city suffered critical water shortages for several days. Consequently, on 6 November 2015, a state of emergency was declared (O.C.D.P. 295/2015) by the National Italian Department of Civil Protection (DPC). During the emergency management phase, a provisional by-pass, consisting of three 350-m long pipes passing through the landslide area, was constructed to restore water to the city. Furthermore, on 11 November 2015, a landslide remote-sensing monitoring system was installed with the following purposes: (i) analyse the landslide geomorphological and kinematic features in order to assess the residual landslide risk and (ii) support the early warning procedures needed to ensure the safety of the personnel involved in the by-pass construction and the landslide stabilization works. The monitoring system was based on the combined use of Ground-Based Interferometric Synthetic Aperture Radar (GB-InSAR) and terrestrial laser scanning (TLS). In this work, the preliminary results of the monitoring activities and a remote 3D map of the landslide area are presented.

Keywords GB-InSAR · Laser scanning · Landslides · Emergency management · 3D mapping

Introduction

Landslides represent one of the most frequent geo-hazards. They represent serious threats to human life and can cause serious socioeconomic losses on the order of billions of Euros, in terms of damage to property, infrastructure and environmental degradation (Kjekstad and Highland 2009; Petley 2012). Recent events show a significant increase in the number of disasters with natural and/or technological causes, and these disasters can have potentially serious consequences for critical infrastructure (CI) (Murray and Grubestic 2007). Where this infrastructure tends to fail or to be destroyed, the resulting cascade effects (chain of events) can lead to catastrophic damage and negative effects on people, the environment and the economy (Geertsema et al. 2009; Kadri et al. 2014). In countries characterized by a geologically young and tectonically active territory, the susceptibility to instability phenomena is further increased. In Italy in particular, approximately 70 % of the country can be considered exposed to landslide risk (<http://www.protezionecivile.gov.it/>) and the related estimated socioeconomic losses range from 1 to 2 billion dollars annually (Canuti et al. 2004). Currently, these values are certainly underestimated.

In the field of landslide detection, mapping, monitoring and management, the availability of advanced remote sensing technologies, which allow the systematic and easily updatable acquisition of data, may enhance the implementation of near-real-

time monitoring activity and the production of landslide maps, optimizing field work (Guzzetti et al. 2012; Frodella et al. 2014). In recent years, the *Ground-Based Interferometric Synthetic Aperture Radar* (GB-InSAR) technique has been widely used to monitor ground displacements in research on landslides (Tarchi et al., 2003; Herrera et al. 2009; Barla et al. 2010; Schulz et al. 2012; Corsini et al. 2013; Bardi et al. 2014), volcanoes (Bozzano et al. 2011; Nolesini et al., 2013; Di Traglia et al. 2014) and sinkholes (Intrieri et al. 2015). *Terrestrial laser scanning* (TLS) has become a widely applied technique for the detection and characterization of several types of mass movements as it allows the rapid collection of detailed and highly accurate 3D ground representations (Abellan et al. 2006; Oppikofer et al. 2008; Jaboyedoff et al. 2009; Fanti et al. 2012; Gigli et al. 2014). The intrinsic characteristics of the abovementioned techniques, such as (i) producing near-real-time displacement maps without physical access to the analysed area; (ii) observing the investigated scenario 24 h per day and in all weather conditions; (iii) generating high-resolution images, especially for analysis of local-scale phenomena; and (iv) providing high versatility and transportability, represent consistent advantages with respect to traditional methods.

This work presents an example of the advantages provided by the integrated use of GB-InSAR and TLS to monitor and manage the post-emergency phase associated with a landslide located in the Catania Province (Sicily Island, Southern Italy). The landslide occurred on 24 October 2015 following intense rainfall that occurred during the previous days (a total of approximately 195 mm measured between 21 and 24 October 2015; data provided by Osservatorio delle Acque—Regione Siciliana) and ruptured a water pipeline that was part of the Messina city aqueduct. Consequently, a considerable lack of water occurred for a large number of the city inhabitants. A provisional by-pass, consisting of three 350-m long pipes passing through the landslide area, was implemented to restore water to the city during the emergency management phase. An integrated monitoring network was also implemented to assess the residual risk by analysing the geomorphological and kinematic features of the landslide and to support the early warning procedures needed to ensure the safety of the personnel involved in the by-pass construction and the long-term landslide stabilization works. The workflow in Fig. 1 explains the organization of the performed activities.

Geological and geomorphological setting

The study area is located in the Calatabiano municipality (Catania Province, Sicily Island), approximately 50 km southwest of the city of Messina and approximately 3 km inland from the Ionian coastline (Fig. 2). From a geomorphologic perspective, the study area is located in the Alcantara River valley, which is delimited to the north by the Peloritani Mountains, to the west by the Nebrodi

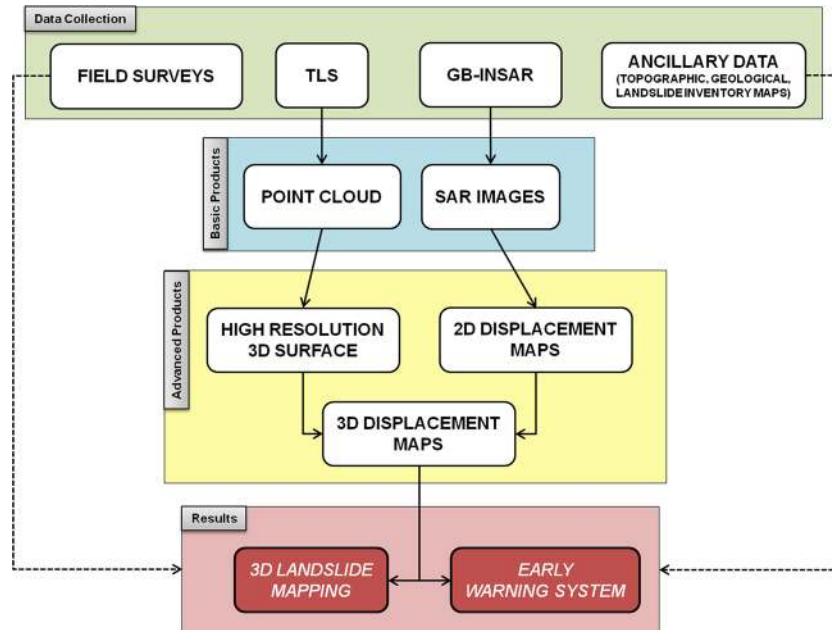


Fig. 1 Logical scheme of the applied operative procedure

Mountains and to the south by the north-eastern slopes of the Etna Volcano (Fig. 2).

The study area is located on the right side of the lowermost Alcantara river alluvial plain and is characterized by hilly terrain ranging from approximately 60 to 250 m a.s.l. The landslide (lat. $37^{\circ} 49' 39''$; long. $15^{\circ} 13' 26''$), which featured a 100-m elevation range and was approximately 110 m in maximum length and 65 m in width, affected a large portion of the east-facing slope overlooking the medieval Calatabiano Castle (Figs. 3 and 4). Its topmost sector is characterized by a wide crown area, where a rotational movement (Cruden and Varnes 1996) occurred, displaying a retrogressive behaviour and almost reached the slope ridge at approximately 200 m a.s.l. The landslide body and toe are affected by minor scarps, while two erosional channels, formed by mud flows that almost reached the creek valley at approximately 100 m a.s.l., border the right and left flanks of the landslide (Figs. 3 and 4). The creek valley is located just a few hundred metres from the northern sector of the inhabited area of Calatabiano and represents a high risk for the local population in case of possible landslide reactivation. The landslide-affected slope is characterized by olive trees, shrubs and rocky scattered outcrops, and field surveys have revealed that the mass movement involved detrital slope deposits a few metres thick and consisting of heterogeneous clasts in a coarse sandy matrix with a small percentage of loam (Fig. 4).

These deposits were formed by the weathering and erosion of the bedrock, represented by the arenaceous-conglomeratic facies (PDT_c) of the Piedimonte Formation (Upper Eocene-Lower Oligocene) (Catalano et al. 2010). This lithofacies is composed of irregular alternations of conglomerates and coarse sandstones. The conglomerate layers present thicknesses of up to 10 m, while the sandstone strata rarely exhibit thicknesses greater than 1 m (Catalano et al. 2010). In the upper part of the slope (Fig. 4), a tectonic thrust contact that erased the original heteropic

succession of the two lithofacies represents the transition to the grey clays lithofacies (PDT_a) of the Piedimonte Formation (Cassola et al. 1991).

Employed remote sensing monitoring techniques

GB-InSAR monitoring

The employed radar system is composed of a coherent microwave transceiver unit operating on the Ku band with a bandwidth of 200 MHz and a central frequency of 17.2 GHz. Synthetic aperture is achieved by moving a motorized sled hosting the radar head along a 3-m long straight rail (parallel to the azimuth direction; Fig. 5a). The working principle of the GB-InSAR technique involves radiating microwaves toward the investigated area and measuring the backscattered signal, obtaining a SAR image. The SAR image is created by combining the spatial resolution along the direction perpendicular to the rail (range resolution; ΔR_r) and the one parallel to the synthetic aperture (azimuth, or cross-range resolution; ΔR_{az}) (Luzi 2010), containing amplitude and phase information of the backscattered echo from the investigated scenario objects.

By evaluating the phase difference, pixel by pixel, between two pairs of averaged sequential SAR images of the same scenario, it is possible to obtain a 2D displacement map of the investigated area, which constitutes an interferogram (Luzi et al. 2004; Monserrat et al. 2014). It is important to note that the system is able to measure only the movement component parallel to the instrument line of sight (L.O.S.—direction connecting the sensor and the investigated object), thus displacements that occur in the direction perpendicular to the sensor are missed. The cross-range resolution depends on the target distance, and good acquisition geometries thus depend on the observed scene. The principal limitations of the GB-InSAR technique are due to temporal decorrelation and atmospheric noise (Luzi et al. 2010).

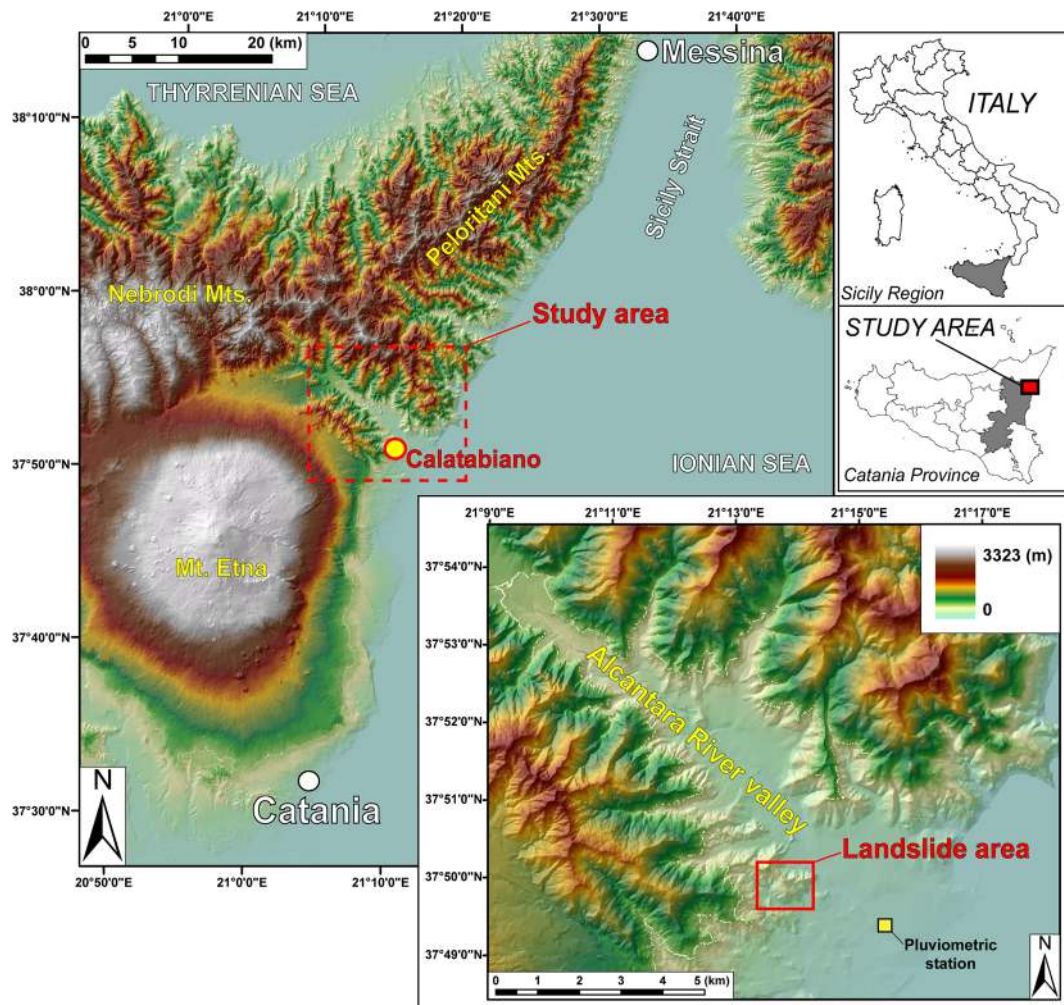


Fig. 2 Study area setting and landslide area location, including the rain gauge station

TLS survey

A TLS device consists of a directional, coherent and in-phase optical beam (or discrete pulses) transmitter, a back-scattered signal receiver and a scanning mechanism (e.g., a rotating mirror). The main product of a long-range laser scanning technique is a high-resolution matrix of points (called a point cloud), defined in polar coordinates (range, horizontal and vertical scanning angle), obtained by measuring the scanner-object distance with great accuracy (on the order of millimetres or centimetres). Given the range distance and the scanning angle, the Cartesian coordinates of each point can be obtained. The high acquisition rate (up to hundreds of thousands of points per second) makes the detailed 3D shape of the object immediately available. Furthermore, for each point, the intensity of the reflected signal is acquired. The intensity data can provide some information about the type of material and the soil moisture content of the targets (Pesci and Teza 2008; Voegtle et al. 2008; Franceschi et al. 2009).

The monitoring system

In the post-landslide event phase, on 11 November 2015, a GB-InSAR system was installed on the terrace roof of the

Calatabiano Castle (Fig. 5a, c). With the aim of optimizing the monitoring system efficiency, the following installation criteria were applied: (i) an adequate sensor-target distance (approximately 500 m), aimed at guaranteeing an azimuth resolution spanning from 40 cm (at 150 m range distance) to 106 cm (at 400 m range distance); (ii) minimum presence of obstacles between the radar sensor and the investigated objects; and (iii) a stable radar location (Fig. 5a). The radar system produces interferograms every 2 min, but cumulative displacement maps can be generated using longer (monthly) temporal baselines to detect both rapid and long-term movements. To obtain a high-resolution 3D surface of the post-event landslide area and to geo-rectify the acquired radar images for a better interpretation of the radar displacement data, TLS surveys were performed on 11 November from the radar system position (Fig. 5a). The employed terrestrial laser scanner is a long-range and high-accuracy 3D time-of-flight instrument (model Riegl LMS-Z420i; RIEGL 2010). This device is able to acquire the position of up to 12,000 points/s by calculating the round-trip travel time of a pulsed laser beam (near-infrared wavelength) from the instrument to the scanned object, with a



Fig. 3 a Image of the Calatabiano landslide acquired on 10 November 2015, from the monitoring system installation point. The *dashed white line* represents the main landslide crown, the *dashed red line* represents the interrupted pipeline (b), and the *black line* represents the new pipeline by-pass (c). P1–P8 represent the GB-InSAR monitoring points

maximum angular resolution of 0.008° , an accuracy of ± 10 mm (one σ at 50 m range under RIEGL test conditions) and from a maximum distance of 800 m (Fig. 5d). The acquired TLS point cloud (approximately 14.5 million points) was linked to a global reference system by performing a GPS survey of 12 laser reflectors placed on the investigated slope. The raw data were subsequently cleared of vegetation, the data points were triangulated, and a 3D mesh was created to produce a continuous surface for the slope.

Results

Monitoring data

The analysed preliminary radar data spans from 11 November to 31 December 2015, when the crucial landslide restoration works and by-pass construction was performed. The logistics of the GB-InSAR system installation provided a good spatial coverage of the landslide-affected area, including its main features (crown, minor scarps, erosional channels) and the pipeline by-pass and bulldozer trails related to the earthworks (Fig. 5). For the monitored site, the cumulative displacement maps were less affected by atmospheric noise than the single interferograms. Therefore, the cumulative displacement maps were considered more suitable for the ground deformation analysis of the slope and for the detection of landslide critical sectors. The detailed cumulative displacement maps are represented with a colour scale visualization: (i) stable areas are shown in light green; (ii) areas characterized by displacement toward the sensor L.O.S. feature colours from yellow to red and purple (maximum cumulative displacement); and (iii) areas characterized by displacements away from the sensor L.O.S. feature colours from dark green to deep blue (Fig. 6).

With the aim of analysing the landslide kinematics, displacement time series were extracted from 8 monitoring points in the displacement maps. These points were selected on the basis of high coherent values of the radar signal and high representativeness of the landslide behaviour (P1–P8) (Figs. 7 and 8). Specifically, the first six points (P1–P6) are located within the landslide body, and their cumulative displacements range from 4.5 mm (P5) up to 83 mm (P1). These points are representative of the areas that showed the highest displacement. The last two points (P7 and P8) were selected in order to be representative of stable areas: they are located outside the landslide body and correspond to a rocky outcrop and a sector of artificial drainage, respectively.

By means of the radar data analysis, a first relevant displacement phase and two further phases after two acceleration events were detected and analysed (Table 1):

- The first 10 days of monitoring activity (11–21 November 2015) show a widespread sector characterized by cumulative displacement values of up to 24 mm (red oval in Fig. 6) corresponding to the upper landslide crown area. Peak cumulative displacements of up to 55 mm are located in small areas in the landslide top-middle and lowermost sectors (white circles in Fig. 6).
- The first phase (after the first acceleration event; 25–26 November 2015) displays 15-mm peak cumulative displacements localized in two restricted areas: the first corresponding to the landslide upper portion (around control point P4) and the second corresponding to the top-middle one (around control point P1) (Fig. 7a).
- The second phase (after the second acceleration event; 22–22 December 2015) exhibits a 15-mm peak cumulative displacement distributed in a widespread area of the landslide top-middle sector (around control points P1–P4) and along the right flank of the slope (Fig. 7b).

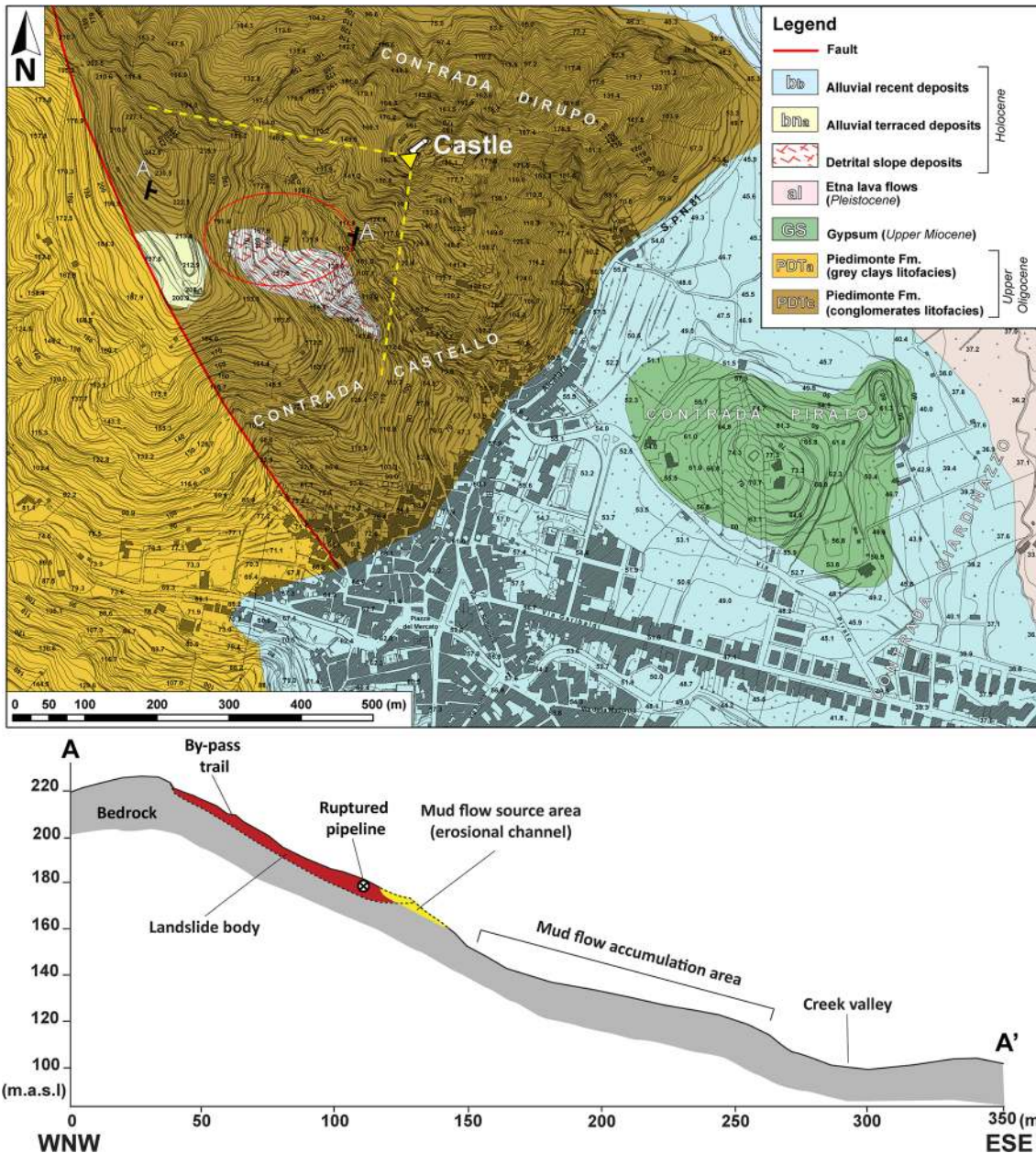


Fig. 4 Geological framework of the landslide area and schematic cross section (red oval highlights the landslide area)

To visualize the detected L.O.S. displacements directly on the 3D representation and therefore better localize the most critical areas of the landslide with respect to the work activities (landslide sectors, pipeline by-pass and bulldozer trails), the GB-InSAR data were merged with the TLS 3D model to obtain a 3D GB-InSAR cumulative displacement map (Fig. 9). Figure 9 displays the selected control points and shows that the maximum cumulative displacements recorded during the monitoring period was approximately 100 mm and occurred near the control point P1.

An early warning procedure was also implemented through the adoption of displacement and velocity thresholds calibrated during the first days of monitoring, when the movements were greatest. A simplified early warning system was developed, based

on three different warning levels: ordinary, pre-alarm and alarm level. To ensure the safety of the workers involved in the restoration works, hourly displacement thresholds were adopted. A change in the level occurred if the following thresholds are surpassed: between 0.5 and 1.0 mm/h for the pre-alarm and >1.0 mm/h for the alarm level. To prevent possible damage to the pipeline by-pass (here representing the CI) and because this slow-moving landslide did not reach high deformation rates, daily displacement thresholds were adopted (between 12 and 24 mm/day for the pre-alarm and >24 mm/day for the alarm level). Communication, which is a fundamental issue of every early warning system (Intrieri et al., 2015), was achieved through the dispatch of monitoring bulletins every 12 h and whenever the warning thresholds were exceeded.

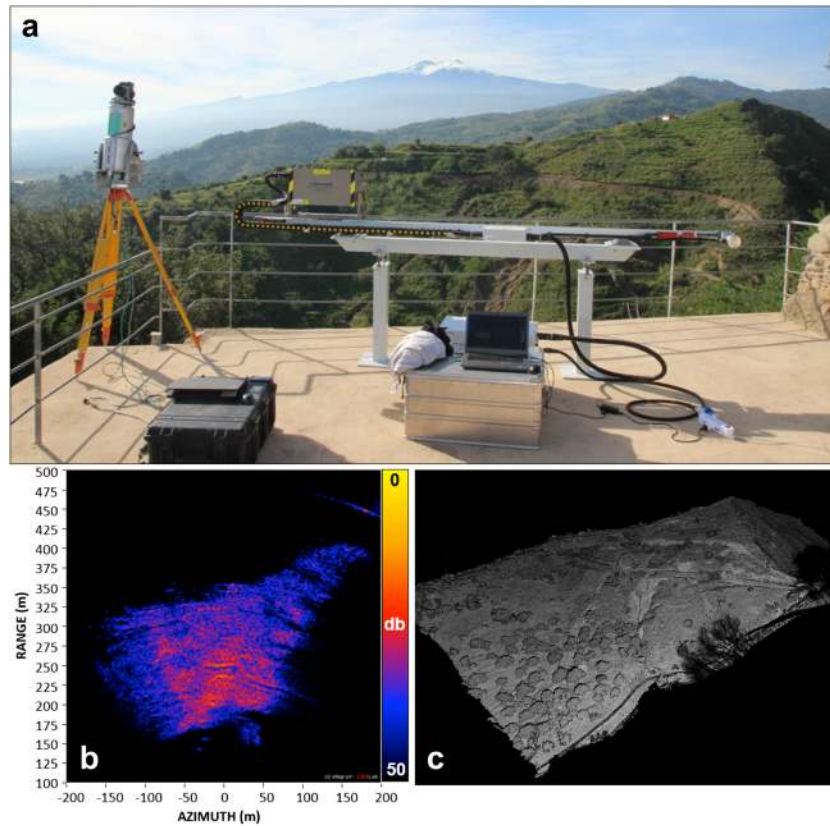


Fig. 5 a Ground-based radar and TLS positioned on the roof of Calatabiano Castle; b power image of the GB-InSAR surveyed slope; c point cloud coloured with intensity values of the reflected laser beam.

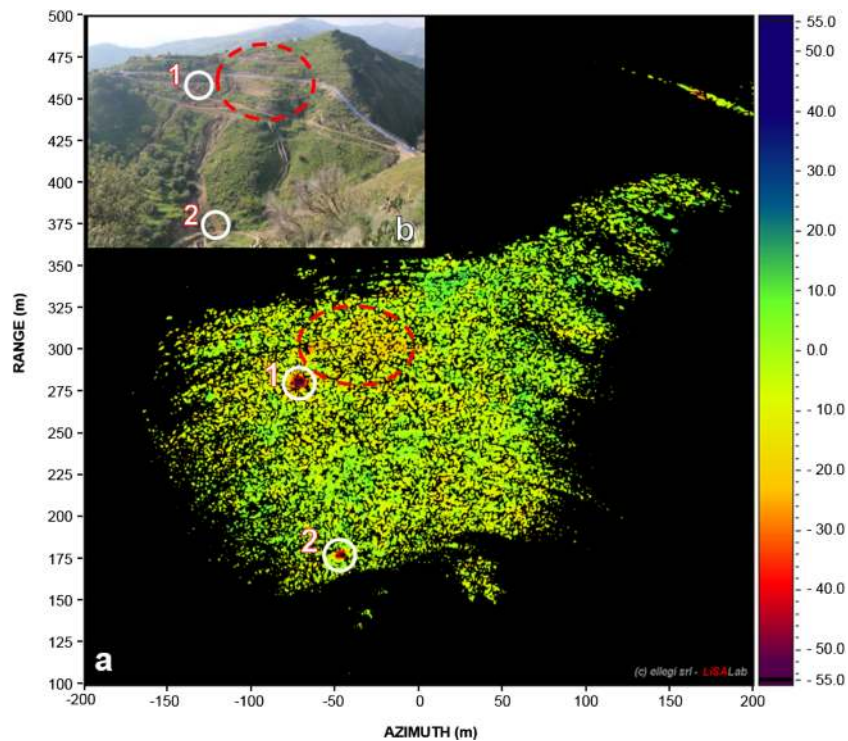


Fig. 6 a Cumulative displacement map obtained by 1 h average interferograms acquired between 11 November 2015 17:59 h GMT + 1 and 21 November 2015 23:00 h GMT + 1 (the *red oval* represents sectors characterized by cumulative displacement values of up to 24 mm, whereas the *white circles* indicate sectors characterized by cumulative peak displacements of up to 55 mm); b corresponding optical image of the landslide scenario acquired on 17 November 2015

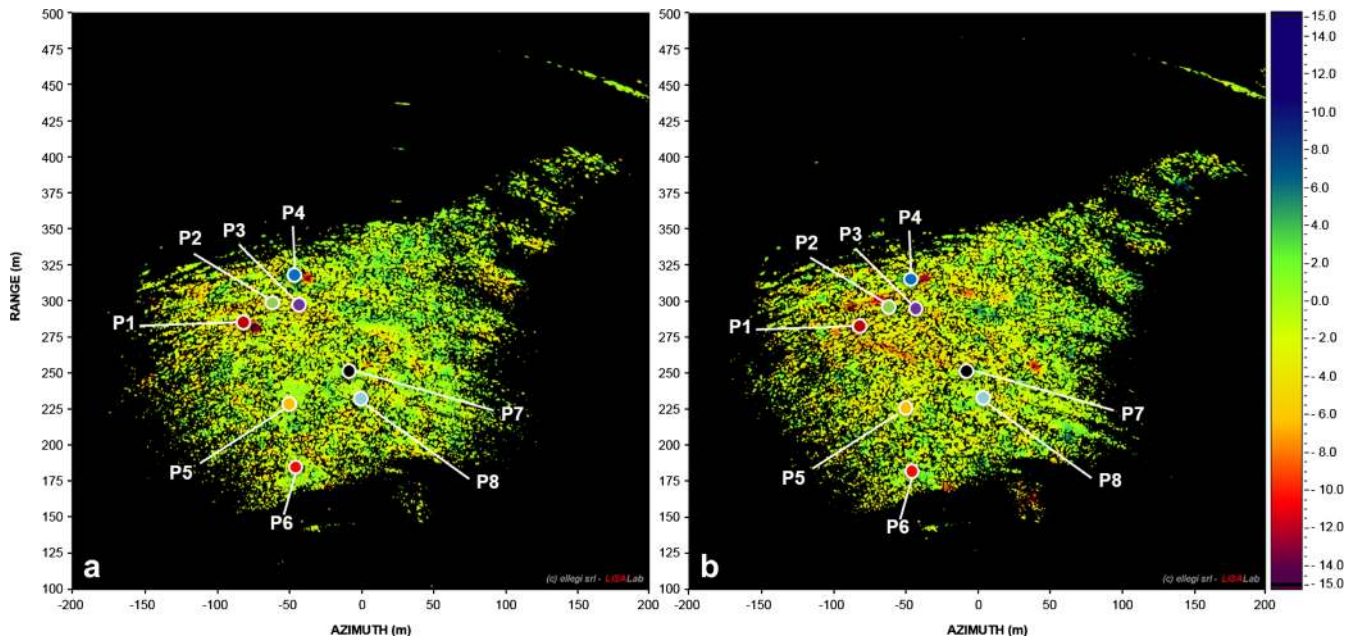


Fig. 7 Cumulative displacement maps obtained based on 1 h averages acquired between a 25 November 2015 05:30 h GMT + 1 and 27 November 2015 17:33 h GMT + 1 and b 20/12/2015 04:59 h GMT + 1 and 22 December 2015 20:12 h GMT + 1. P1-P8 represent the GB-InSAR monitoring points

Remote 3D mapping

The high-resolution point cloud and the variable laser return intensity values also allowed us to add information regarding

the main geomorphologic features of the landslide. In fact, the raw laser scanner product (Fig. 10) shows high intensity values in association with bare soils and rock outcrops. In contrast, the

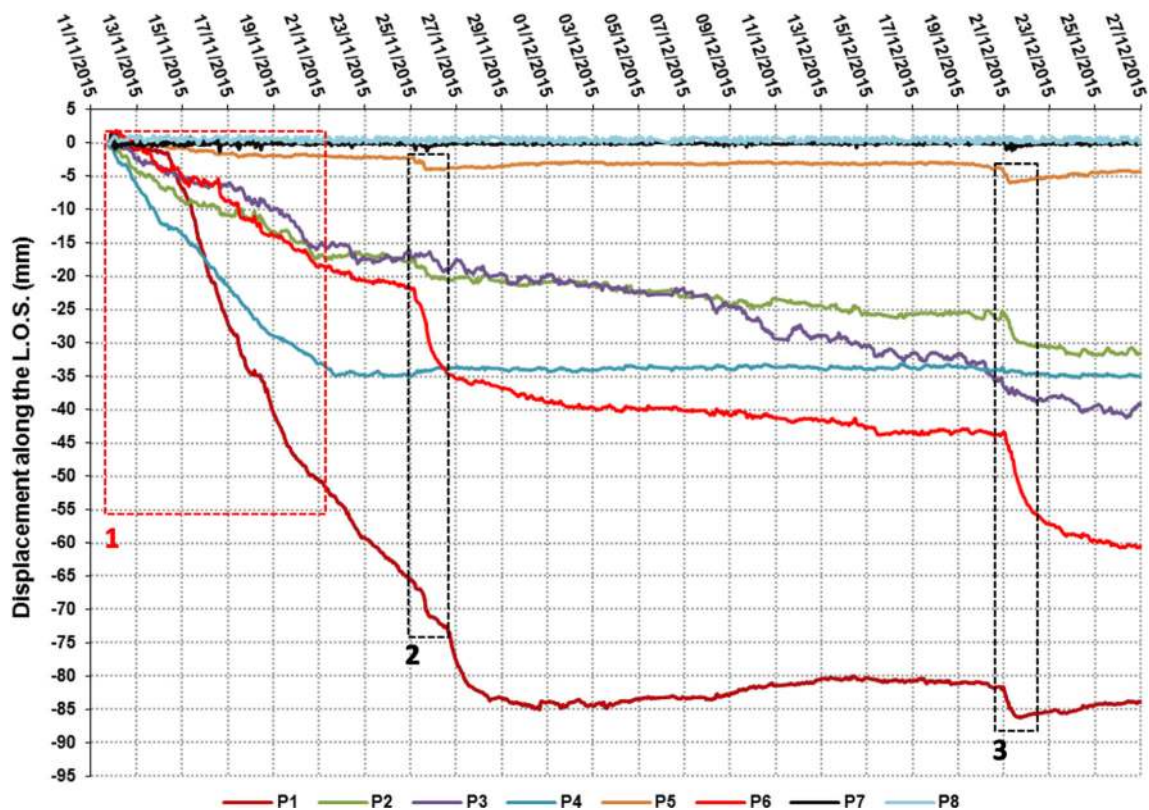


Fig. 8 Time series of GB-InSAR monitoring points (*dotted red rectangle* highlights the detected displacement phase: 1 = first 10 days of monitoring; *dotted black rectangles* denote the phases after the two acceleration events: 2 = first period, 3 = second period).

Table 1 Analysed cumulative displacement (in mm) and acceleration events (mean velocity in mm/day) of the GB-InSAR control points

Time period	Elapsed hours	Point 1 displacement (velocity)	Point 5 displacement (velocity)	Point 6 displacement (velocity)
11 Nov. 2015 17:59–21 Nov. 2015 23:03	244	54.3 (0.22)	2.1 (0.01)	19.6 (0.08)
25 Nov. 2015 02:25–26 Nov. 2015 17:00	37	7.6 (0.19)	1.6 (0.04)	12.8 (0.35)
20 Dec. 2015 23:43–22 Dec. 2015 20:12	45	3.7 (0.08)	0.9 (0.02)	13.7 (0.31)

erosional channel thalwegs of the landslide are characterized by low intensity values, probably due to the moisture influencing the backscattered signal through absorption of the near-infrared wavelength beam (Franceschi et al. 2009). However, it is important to highlight that the difference in intensity values depends on several factors, such as the acquisition geometry (e.g. scanner-object distance and angle of incidence; Kaasalainen et al. 2011), the surface roughness and the presence of vegetation. The TLS point cloud was also used to validate the location of the selected GB-InSAR control points with respect to the landslide geomorphological features: right flank erosional channel topmost sector (P1), by-pass pipes trail (P2, P3), upper crown sector (P4), left flank erosional channel source area (P5), lowermost sector (P6), rock outcrop (P7) and upper sector of the artificial drainage (P8).

Discussion

The main outcomes of this work suggest the effectiveness of the integrated monitoring system adopted to manage the Calatabiano landslide post-emergency phase. The peculiarity of this landslide event was its severe damage to CI, here represented by the disrupted local aqueduct, which produced a water shortage crisis in the city of Messina that lasted for several days and caused problems and discomfort for the local

population. The adopted approach gave priority to a rapid system installation and near-real-time monitoring, in order to rapidly detect landslide displacements, ensure the safety of the workers involved in both the water pipeline by-pass construction and the landslide stabilization works and avoid further possible damage to the CI. Thanks to the versatility and portability of the devices, the GB-InSAR system was installed in a few hours on 11 November 2015, and the first displacement data became available while the TLS survey was performed. Furthermore, the employed remote sensing technique integration proved to be effective in surveying and monitoring the whole slope, overcoming the limitations of traditional single-point measurements.

The first 10 days of monitoring (11–21 November 2015; Figs. 6 and 8, Table 1) recorded the highest deformation rates (phase 1), which were related to the residual displacement of the landslide following the initial failure. As shown in Fig. 11, the landslide trigger was clearly related to the rainfall events that preceded on 24 October. In particular, more than 195 mm of cumulative precipitation fell during the period between 21 and 24 October (of which 182 mm occurred solely on 22 October).

Another rainfall event occurred between 30 October and 3 November (a total of 130 mm of cumulative precipitation was recorded, with a daily peak of 90 mm on 2 November; Fig. 11).

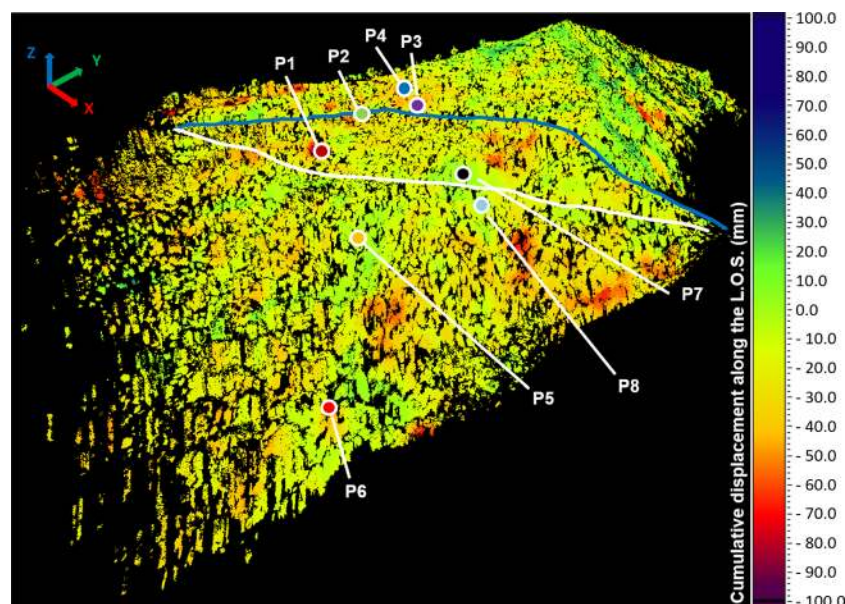


Fig. 9 Cumulative 3D displacement map for the entire monitoring period (from 11 November to 31 December 2015). GB-InSAR monitoring points (P1-P8) are highlighted together with the pipeline by-pass trail (blue line) and the bulldozer trail (white line)

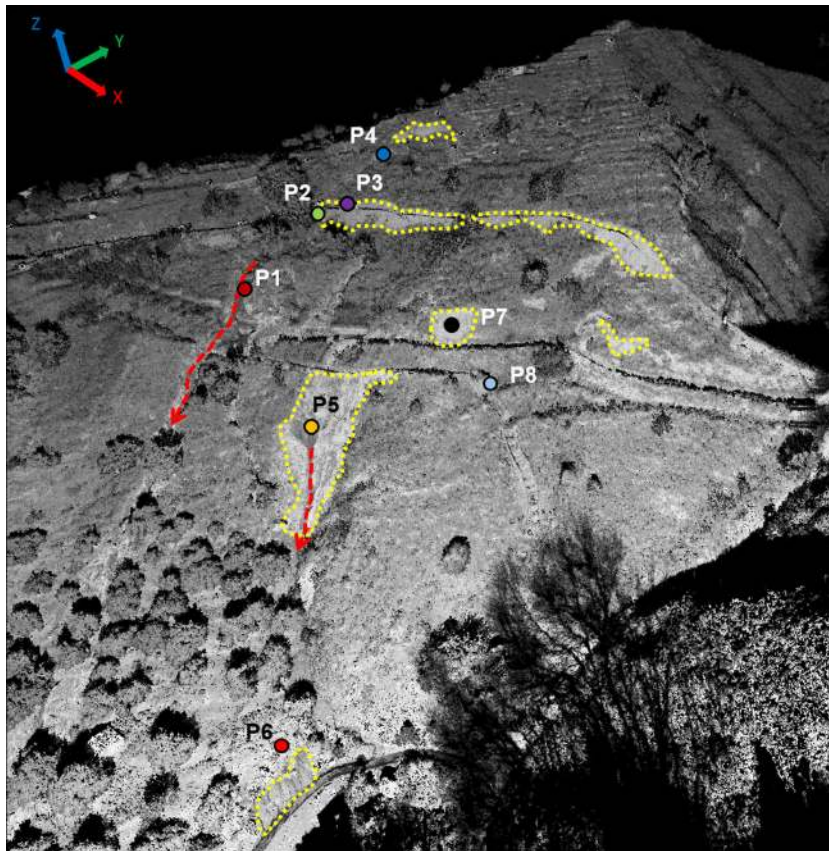


Fig. 10 TLS point cloud shaded by intensity values and GB-InSAR control points. *Yellow dashed polygons* indicate high intensity values related to bare soils and rock outcrops, corresponding to the following slope sectors, from top to bottom: the landslide crown, the by-pass pipes trail, the left bank erosional channel source area and the lowermost sector. The *red lines* mark the thalwegs of the erosion channels. P1–P8 represent the GB-InSAR monitoring points

This event may have contributed to the deformational trend. Two additional, albeit less intense, displacement periods (phases 2 and 3) were recorded during 25–26 November 2015 and 20–22

December 2015 (Figs. 7 and 8, Table 1), coinciding with two less intense rainfall events (approximately 25 and 30 mm of cumulative recorded precipitation, respectively) (Fig. 11). While the

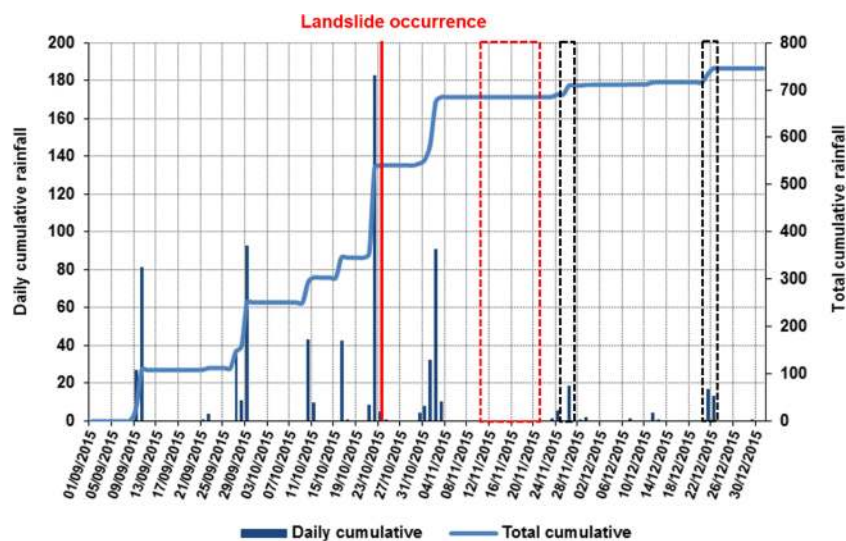


Fig. 11 Rainfall data from the Alcantara rain gauge station (courtesy of Osservatorio delle Acque—Regione Siciliana). *Dashed rectangles* indicate the first 10 days of monitoring (in red) and the phases after two further acceleration events (in black)

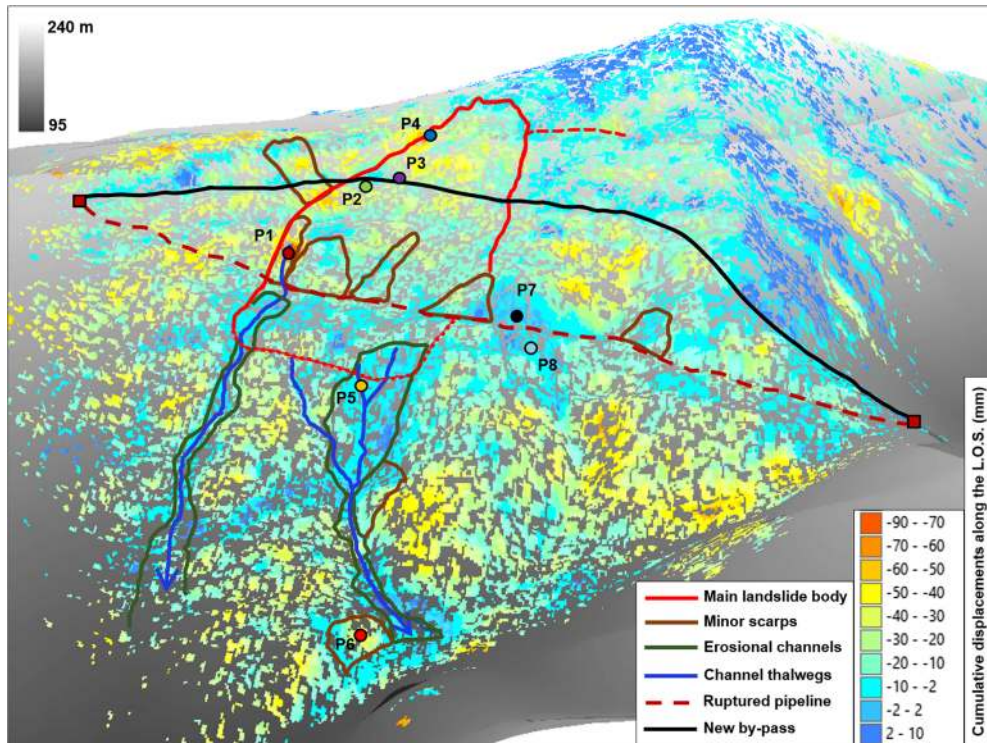


Fig. 12 3D geomorphological map of the Calatabiano landslide, projected on a high-resolution DEM, obtained by means of the TLS survey, and on the GB-InSAR cumulative displacement map. Control points, the pipeline by-pass trail (*black line*) and the ruptured pipeline (*dashed red line*) are highlighted. *P1–P8* represent the GB-InSAR monitoring points

first displacement phase (particularly evident in the *P1* and *P4* control points time series) shows the features of post-landslide residual deformation, the second and third phases (particularly

evident in the *P1*, *P5* and *P6* control points series; Fig. 8) were associated with impulsive acceleration events that were very similar in terms of magnitude and elapsed time (Table 1).

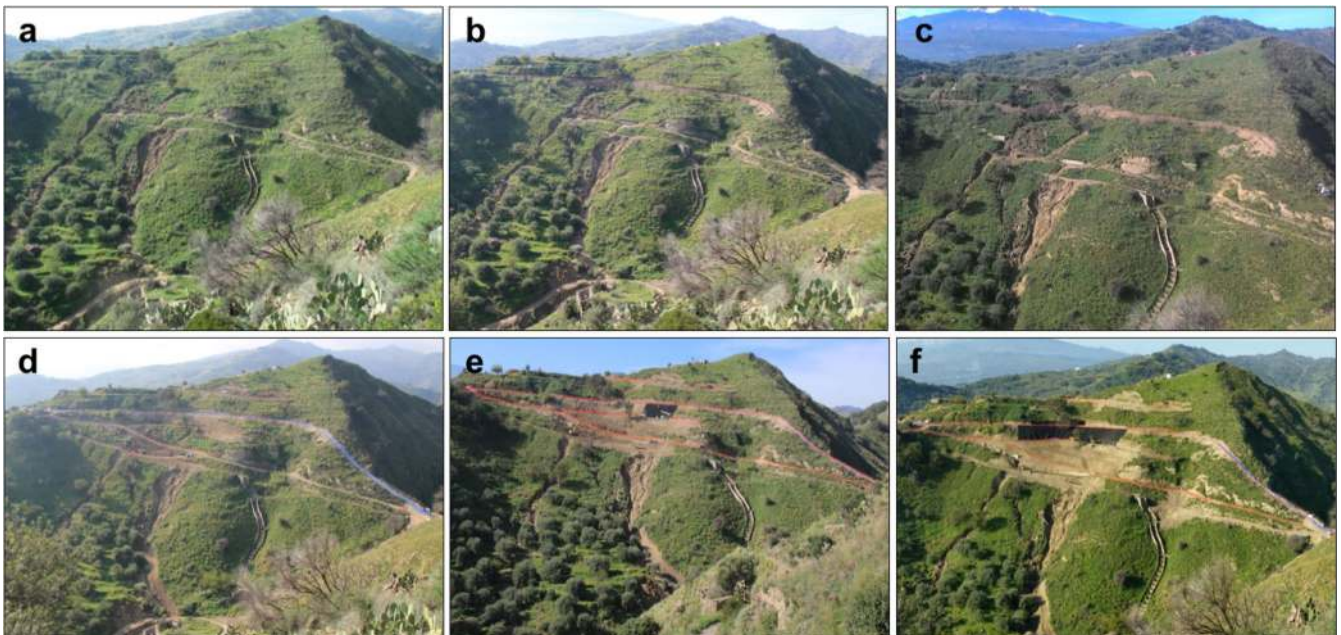


Fig. 13 Evolution of the earthworks on the monitored slope: *a, b* by-pass trail construction (10–12 November); *c, d* beginning of the slope reprofiling and by-pass pipe emplacement (14–17 November); *e, f* geogrid positioning and intense slope reprofiling (21 November–27 December)

The interpretation of the remote sensing data collected from 11 November to 31 December 2015 was supported by means of the remote 3D products (Figs. 9 and 10). Furthermore, these 3D products were integrated to generate an accurate 3D geomorphological map of the landslide (Fig. 12), with the aims of accurately locating the recorded displacements with respect to the landslide geomorphological features and the excavation activities and detecting critical sectors on the monitored slope. The following areas were determined to be critical sectors:

- The uppermost area of the right flank erosional channel, which during the monitored period was affected by high and constant displacements (Figs. 6, 7a and 9), as confirmed by the control point P1 time series (Fig. 8)
- The left flank erosional channel source (control point P5 area) and lowermost sectors (control point P6 area) (minor scarp in Fig. 12). The latter sector proved to be one of the most active in the first 10 days of monitoring (Fig. 6), as displayed by the P6 cumulative displacement (approximately 62 mm, the second highest value within the control points). Corresponding to the erosional channels, the time series of control points P1, P5 and P6 clearly show the presence of displacement, probably induced by the high ground moisture content, as confirmed by the rainfall data (Fig. 11) and field inspections
- The landslide upper crown area (control point P4 area), which was largely involved in the residual deformation observed during the first 10 days of monitoring (Fig. 6)
- The by-pass pipes (located in the area of control points P2 and P3), displaying 32 and 39 mm of cumulative displacement, respectively (Figs. 8 and 9)
- Monitored slope areas located outside the landslide body, corresponding to both the earth movement associated with the excavation of the by-pass and bulldozer trails and the landslide slope re-profiling (Figs. 7 and 13).

The main limitations of the GB-InSAR displacement data interpretation included noise effects and temporal decorrelation, due to the widespread vegetation cover of the monitored slope and the influence of man-made excavations and earth movement related to the by-pass construction and landslide restoration works. Therefore, the remotely sensed data were validated by means of periodic field inspections (Fig. 13), which proved to be crucial in detecting and interpreting the evolution phases of the construction during the monitoring period, especially for the bulldozer trails and slope reprofiling area (Figs. 7b and 13d–f).

The 3D landslide geomorphological map was fundamental in understanding the kinematic mechanisms associated with the landslide mass and in assessing the areal distribution of the landslide (a total of approximately 4900 m²) and its volume (on the order of approximately 25,000 m³, considering a 5-m average thickness of the landslide body based on field surveys). Therefore, accurate mapping provided important information for the local authorities and technicians involved in the emergency management and in the restoration works.

Conclusions

On 24 October 2015, intense rainfall triggered a landslide north of the town of Calatabiano (Sicily Island, Southern Italy). Although the

portion of the slope affected by the failure was not exceptional in size or volume and no human casualties occurred, the event had an enormous social impact. The major pipeline providing water to the city of Messina was disrupted, and approximately 80 % of the city had limited access to this vital service for several days. The event demonstrated how the risk associated with landslides should not be assessed and managed only in terms of human safety but also in terms of the vulnerability of critical infrastructure. The remediation works required the creation of a by-pass trail around the damaged pipeline section and had to be performed directly on the unstable slope. Therefore, to assess the safety of the workers, a fully operational real-time monitoring network was deployed. The integrated use of GB-InSAR and TLS techniques allowed for a complete landslide characterization and a continuous assessment of the ongoing deformation rates on the slope. Two displacement thresholds and two velocity thresholds were defined in agreement with the emergency plan, which was based on a scale with three different warning levels. The triggering of the landslide was related to the rainfall events that preceded 24 October 2015, and the two accelerations recorded during the monitoring period (from 10 November to 31 December 2015) were correlated with the amount of precipitation in the area.

Acknowledgments

The authors would like to thank the following groups for their support during the post-landslide emergency phase: the National Department of Civil Protection (DPCN), the Sicilian Regional Department of Civil Protection (DPCR) and the appointed Commissioner-Delegate, as well as the Osservatorio delle Acque—Regione Siciliana for providing rainfall data.

The GB-InSAR apparatus used in this application was designed and produced by Ellegi s.r.l. and was based on the proprietary technology GB-InSAR LiSALAB derived from the evolution and improvement of LiSA technology licenced by the Ispra Joint Research Centre of the European Commission.

Open Access This article is distributed under the terms of the Creative Commons Attribution 4.0 International License (<http://creativecommons.org/licenses/by/4.0/>), which permits unrestricted use, distribution, and reproduction in any medium, provided you give appropriate credit to the original author(s) and the source, provide a link to the Creative Commons license, and indicate if changes were made.

References

- Abellan A, Vilaplana JM, Martinez J (2006) Application of a long-range terrestrial laser scanner to a detailed rockfall study at Vall de Nuria (eastern Pyrenees, Spain). *Eng Geol* 88:136–148
- Bardi F, Frodella W, Ciampalini A, Bianchini S, Del Ventisette C, Gigli G, Fanti R, Moretti S, Basile G, Casagli N (2014) Integration between ground based and satellite SAR data in landslide mapping: the san Fratello case study. *Geomorphology* 223:45–60
- Barla G, Antolini F, Barla M, Mensi E, Piovano G (2010) Monitoring of the Beauregard landslide (Aosta Valley, Italy) using advanced and conventional techniques. *Eng Geol* 116:218–235
- Bozzano F, Cipriani I, Mazzanti P, Prestininzi A (2011) Displacement patterns of a landslide affected by human activities: insights from ground-based InSAR monitoring. *Nat Hazards* 59:1377–1396
- Canuti P, Casagli N, Ermini L, Fanti R, Farina P (2004) Landslide activity as a geoinicator in Italy: significance and new perspectives from remote sensing. *Environ Geol* 45(907):919
- Cassola P, Giammarino S, Puglisi D, Villa G (1991) Nuovi dati sedimentologico-petrografici e biostratigrafici sulla formazione di Piedimonte (Sicilia nord-orientale). *Mem Soc Geol Ital* 47:213–223

- Catalano S, Corsaro RA, Marino M, Branca S, Cirrione R, De Guidi G, Di Stefano A, Mazzoleni P (2010) Note illustrative della Carta Geologica d'Italia alla scala 1:50000, Foglio 613, Taormina. Ispra, S. EL. Ca, Firenze
- Corsini A, Berti M, Monni A, Pizziolo M, Bonacini F, Cervi F, Ciccarese G, Ronchetti F, Bertacchini E, Capra A, Gallucci A, Generali M, Gozza G, Pancioli V, Pignone S, Truffelli G (2013) Rapid assessment of landslide activity in Emilia Romagna using GB-InSAR short surveys. In: *Landslide science and practice*. Springer, Berlin Heidelberg, pp. 391–399
- Cruden DM, Varnes DJ (1996) Landslides types and processes. In: Turner AK, Schuster RL (eds) *Landslides: investigation and mitigation*. Transportation Research Board special report 247. National Academy Press, WA, pp. 36–75
- Di Traglia F, Nolesini T, Intrieri E, Mugnai F, Leva D, Rosi M, Casagli N (2014) Review of ten years of volcano deformations recorded by the ground-based InSAR monitoring system at Stromboli Volcano: a tool to mitigate volcano flank dynamics and intense volcanic activity. *Earth-Sci Rev* 139:317–335
- Fanti R, Gigli G, Lombardi L, Tapete D, Canuti P (2012) Terrestrial laser scanning for rockfall stability in the cultural heritage site of Pitigliano (Italy). *Landslides* 5:1–12
- Franceschi M, Teza G, Preto N, Pesci A, Galgaro A, Girardi S (2009) Discrimination between marls and limestones using intensity data from terrestrial laser scanner. *ISPRS J Photogramm* 64:522–528
- Frodella W, Morelli S, Fidinoli F, Pazzi V, Fanti R (2014) Geomorphology of the Rotolon landslide (Veneto region, Italy). *Journal of Maps* 10(3):394–401
- Geertsema M, Schwab JW, Blais-Stevens A, Sakals ME (2009) Landslides impacting linear infrastructure in west Central British Columbia. *Nat Hazards* 48:59–72
- Gigli G, Intrieri E, Lombardi L, Nocentini M, Frodella W, Balducci M, Venanti LD, Casagli N (2014) Event scenario analysis for the design of rockslide countermeasures. *J Mt Sci* 11(6):1521–1530
- Guzzetti F, Mondini AC, Cardinali M, Fiorucci M, Santangelo M, Chang KT (2012) Landslide inventory maps: new tools for an old problem. *Earth-Sci Rev* 112:1–25
- Herrera G, Fernández-Merodo JA, Mulas J, Pastor M, Luzi G, Monserrat O (2009) A landslide forecasting model using ground based SAR data: the Portalet case study. *Eng Geol* 105:220–230
- Intrieri E, Gigli G, Nocentini M, Lombardi L, Mugnai F, Fidinoli F, Casagli N (2015) Sinkhole monitoring and early warning: an experimental and successful GB-InSAR application. *Geomorphology* 241:304–314
- Jaboyedoff M, Oppikofer T, Locat A, Locat J, Turmel D, Robitaille D, Demers D, Locat P (2009) Use of ground-based LIDAR for the analysis of retrogressive landslides in sensitive clay and of rotational landslides in river banks. *Can Geotech J* 46:1379–1390
- Kaasalainen S, Jaakkola A, Kaasalainen M, Krooks A, Kukko A (2011) Analysis of incidence angle and distance effects on terrestrial laser scanner intensity: search for correction methods. *Remote Sens* 3:2207–2221
- Kadri F, Birregah B, Châtelet E (2014) The impact of natural disasters on critical infrastructures: a domino effect-based study. *J Homel Secur Emerg* 11:217–241
- Kjekstad O, Highland L (2009) Economic and social impacts of landslides. In: *Landslides—disaster risk reduction*. Springer, Berlin Heidelberg, pp. 573–587
- Luzi G (2010) Ground based SAR interferometry: a novel tool for geoscience. INTECH Open Access Publisher
- Luzi G, Pieraccini M, Mecatti D, Noferini L, Guidi G, Moia F, Atzeni C (2004) Ground-based radar interferometry for landslides monitoring: atmospheric and instrumental decorrelation sources on experimental data. *IEEE T Geosci Remote* 42:2454–2466
- Monserrat O, Crosetto M, Luzi G (2014) A review of ground-based SAR interferometry for deformation measurement. *ISPRS J Photogramm* 93:40–48
- Murray AT, Grubestic TH (2007) Overview of reliability and vulnerability in critical infrastructure. In: *Critical Infrastructure*. Springer, Berlin Heidelberg, pp. 1–8
- Nolesini T, Di Traglia F, Del Ventisette C, Moretti S, Casagli N (2013) Deformations and slope instability on Stromboli Volcano: integration of GBInSAR data and analog modeling. *Geomorphology* 180:242–254
- Oppikofer T, Jaboyedoff M, Blikra LH, Derron MH (2008) Characterization and monitoring of the Aknes rockslide using terrestrial laser scanning. *Proceedings of the 4th Canadian conference on geohazards: from causes to management*, pp. 211–218
- Pesci A, Teza G (2008) Effects of surface irregularities on intensity data from laser scanning an experimental approach. *Ann Geophys-Italy* 51:839–848
- Petley D (2012) Global patterns of loss of life from landslides. *Geology* 40:927–930
- RIEGL (2010) Data sheet of long range & high accuracy 3D terrestrial laser scanner LMS-Z420i. http://www.riegl.com/uploads/tx_pxpriegl/downloads/10_DataSheet_Z420i_03-05-2010.pdf
- Schulz WH, Coe JA, Shurtleff BL, Panosky J, Farina P, Ricci PP, Barsacchi G (2012) Kinematics of the Slumgullion landslide revealed by ground-based InSAR surveys. In *Proc. Landslides and Engineered Slopes: Protecting Society through Improved Understanding—the 11th International and 2nd North American Symposium on Landslides and Engineered Slopes*, Banff, Canada, pp. 3–8
- Tarchi D, Casagli N, Fanti R, Leva D, Luzi G, Pasuto A, Pieraccini M, Silvano S (2003) Landslide monitoring by using ground-based SAR interferometry: an example of application to the Tessina landslide in Italy. *Eng Geol* 68:15–30
- Voegtli T, Schwab I, Landes T (2008) Influences of different materials on the measurements of a Terrestrial Laser Scanner (TLS). *The International Archives of the Photogrammetry, Remote Sensing and Spatial Information Sciences*. Vol. XXXVIII. Part B5. Beijing

L. Lombardi · M. Nocentini · W. Frodella · T. Nolesini · F. Bardi · E. Intrieri · T. Carlià · L. Solari · G. Dotta (✉) · F. Ferrigno · N. Casagli

Department of Earth Sciences,
University of Firenze,
Via La Pira 4, 50121, Florence, Italy
e-mail: giulia.dotta@unifi.it

T. Carlià · L. Solari · G. Dotta
Regional Doctoral School of Earth Sciences,
University of Firenze,
Via La Pira 4, 50121, Florence, Italy